ARCHIVE OF APPLIED MECHANICS

https://www.springer.com/journal/419

Impact factor = 1.976

Accepted June 22nd 2022

UNSTEADY SQUEEZING FLOW OF A MAGNETIZED DISSIPATIVE NON-NEWTONIAN NANOFLUID WITH RADIATIVE HEAT TRANSFER AND FOURIER-TYPE BOUNDARY CONDITIONS: NUMERICAL STUDY

J. C. Umavathi[1*], K. Vajravelu[2], O. Anwar Bég[3] and Umar F. Khan[4]

[1]Department of Mathematics, Gulbarga University, Gulbarga-585 106, Karnataka, ***INDIA.***

[2]Department of Mathematics, University of Central Florida, Orlando, Florida 32816, ***USA.***

[3]Multi-Physical Engineering Sciences Group, Aeronautical/Mechanical Engineering, Salford University, School of Science, Engineering and Environment (SEE), Manchester, M54WT, ***UK.***

[4] Magnetic Materials, School of Engineering, Robert Gordon University, Garthdee Road, Aberdeen AB10 7GE, ***Scotland.***

****Corresponding author- email:*** *drumavathi@rediffmail.com; co-authors- O.A.Beg@salford.ac.uk; u.khan@rgu.ac.uk*

Abstract: Improved thermal management in high temperature tribological systems requires novel developments in lubricants. Motivated by combining nanoparticle and magnetorheological plastomer (MRP) features, this research paper deals with the analysis of the high-temperature magnetohydrodynamic squeeze flow of a Casson nanofluid between parallel disks with the Fourier-type boundary conditions including radiation. Rosseland's diffusion flux and the Buongiorno nanoscale model are used. Suction and injection effects at the disks are also considered as is viscous heating. Robin (Fourier) boundary conditions are included and the Buongiorno nanoscale model is used which enables the simulation of nanoparticle mass diffusion, Brownian motion and thermophoresis. The emerging nonlinear boundary value problem is solved with the bvp4c routine in MATLAB routine with appropriate boundary conditions at the disks. The effects of squeeze number, Hartmann number, Brownian motion parameter, Prandtl number, Eckert number, thermophoresis parameter, Casson viscoplastic rheological parameter and thermal radiation parameter for both disk suction and injection cases and also with *equivalent and different* Biot numbers at the disks, are presented graphically. MATLAB solutions are validated with earlier published results. Drag force increases with greater magnetic field strength. Increasing squeezing parameter substantially modifies the velocity distribution causing a deceleration near the disk surfaces but an acceleration further from the disks. Elevation in Prandtl number and Eckert number results in a significant enhancement in temperature but a strong depletion in nanoparticle concentration for both equal and unequal Biot numbers at the disk surfaces. Nanoparticle concentration is depleted at the disk surfaces with increasing Brownian motion parameter values. With an increase in the Casson viscoplastic parameter, temperature decreases i. e. cooling is induced, whereas nanoparticle concentration increases. The simulations show that significant temperature elevation is produced with increasing Brownian diffusion, viscous dissipation and radiative flux effects and that combining nanoparticles and viscoplastic effects offers a good thermal management mechanism in squeezing lubrication.

Keywords: *Thermal radiation; Heat Transfer; Casson nanofluid; Parallel disks; Fourier-type boundary conditions; Magnetohydrodynamic squeezing flow; MATLAB; Lubrication*.

Nomenclature:

A	Suction/ Blowing parameter
B	Strength of magnetic field
B_0	Strength of magnetic field
Cfr	Skin friction coefficient
Bi_1, Bi_2	Biot number
D_T	Thermophoretic diffusion coefficient
D_B	Brownian motion coefficient
Le	Lewis Number
a, H	Positive constants
k	Thermal conductivity
S	Squeeze number
Nt	Thermophoresis parameter
Nb	Brownian motion parameter
Nur	Nusselt number
Shr	Sherwood number
$h(t)$	Distance between the two disks
Nu	Nusselt number
Pr	Prandtl Number
P	Pressure
r / z	Space coordinate
T	Temperature
C	Concentration
C_h	Concentration at the upper disk
C_w	Concentration at the lower disk
u, w	Velocity components
w_0	Suction/blowing velocity
T_h	Temperature at the upper disk
T_w	Temperature at the lower disk

T_m Mean fluid temperature

M Hartmann number

Re_r Reynolds number

C_p Specific heat

f Dimensionless stream function

q_w Surface heat flux

Green Number:

η Similarity variable

τ Heat capacity

α Thermal diffusivity

μ Dynamic Viscosity

σ Electric conductivity

β Casson non-Newtonian parameter

ρ Density

θ Dimensionless Temperature

ϕ Dimensionless Concentration

υ Kinematic viscosity

1. Introduction

Squeezing flow is of fundamental interest in engineering sciences and applications include radial diffusers, turbine engines, rotating wafers, bearing system lubrication, aircraft landing gear, automotive shock absorbers, hydraulic lifts etc. Such flows often feature multiple physical effects including heat transfer, mass transfer, unsteadiness, electromagnetics, lubricant rheology etc. Many diverse studies of such flows have been communicated including Çelik and Öztürk [1] (on thermal squeezing), Kang *et al.* [2] (on magnetic squeeze film dampers), McIClark [3] (on slurry squeezing dynamics), Bég *et al.* [4] (orthopaedic magneto-tribology), Naduvinamani *et al.* [5] (machine bearings), Bhat and Deberi [6] (annular magnetic plate lubrication) and Lin *et al.* [7] (squeeze-film air bearings). Such fluids also offer attractive properties for anti-corrosion and

anti-oxidation protection, prolonged working life and boosted heat dissipation which are key aspects of modern lubrication engineering. Walters [8] highlighted the superior load journal-bearing performance of non-Newtonian liquids (e.g. viscoelastic multigrade oils) identifying the relaxation time and enhanced pressure dependence as key beneficial factors. Non-Newtonian fluids require a nonlinear relationship between stress and strain and the Newtonian classical viscous flow model can be retrieved as a special case. They include paints, gels, greases, mineral oils, synthetic oil, silicon fluids, polymers etc. Various mathematical models have been employed to simulate the squeezing flows of non-Newtonian fluids which may also be electrically conducting (magnetic polymer lubricants). Ohno and Hirano [9] confirmed the many advantages of non-Newtonian lubricants (e.g. viscoplasticity, viscoelasticity, relaxation and retardation) Motivated by the superior performance of rheo-lubricants, many analytical and computational investigations of non-Newtonian squeeze film flows have appeared in recent years. Hayat *et al.* [10] used a homotopy method to derive convergent series solutions for magnetohydrodynamic squeezing flow of a third grade Reiner-Rivlin viscoelastic fluid between approaching disks with Joule and viscous heating effects. Muravleva [11] derived asymptotic solutions for the axisymmetric squeeze flow of a viscoplastic fluid, identifying a pseudo-plug region in which the leading order equation predicts a plug and deploying a slip yield boundary condition at the disks. Xu *et al.* [12] studied theoretically and experimentally the squeeze flow behaviors (including compressive, tensile, and oscillatory squeeze behaviors) of magnetorheological plastomers (MRPs), noting that magnetic field, particle distribution, and particle concentration significantly modify the stress and flow behaviour and that MRPS significantly outperform conventional lubricants. Phan-Thien and Walsh [13] derived similarity solutions for squeezing flow of an Oldroyd-B viscoelastic fluid. Muravlev [14] conducted both asymptotic and numerical studies (accelerated proximal gradient and augmented Lagrangian methods) of the axisymmetric squeeze flow of a viscoplastic Casson fluid using no-slip and slip yield boundary conditions at the wall. Shamshuddin *et al.* [15] used both MATLAB and the successive Taylor series linearization method (STSLM) with Chebyshev interpolating polynomials and Gauss-Lobatto collocation, to analyze the mixed bioconvection magnetohydrodynamic squeezing flow with first order homogenous destructive chemical reaction between parallel plates. Çelik and Öztürk [16] discussed the squeezing flows between parallel disks, of which one disk is impermeable and the other is porous, in the presence of

magnetic field using Gegenbauer Wavelet Collocation Method (GWCM). GWCM is generalized form of the Legendre, Chebyshev and second kind Chebyshev wavelets. From the numerical results, it was observed that GWCM was convergent even in the case of a small number of grid points. Heat transfer and entropy generation due to laminar natural convection in a square cavity filled with non-Newtonian nanofluid was analyzed by Kefayati [17] using Finite Difference Lattice Boltzmann Method. It was concluded that the augmentation of the power-law index caused heat transfer to drop while increase in volume fraction of nanoparticles augmented it. Entropy generation due to fluid friction and heat transfer was rised as Rayleigh number enhanced.

The above studies did not consider *high temperature lubrication*. In a number of squeezing flows, excessive heat buildup within the bearing is one of the main factors that can warn of impending failure. In extreme cases radiative heat transfer is invoked. This has been observed in railroad catastrophic bearing failure [18] where engineers have identified that neglection of radiative heat effects (generally observed above 150 Celsius) leads to premature thermal damage of the bearing system. Body-to-body radiation arises, and this necessitates the inclusion of radiative heat flux in mathematical models. Such models may also feature complex boundary conditions for ambient temperature, emissivity etc [19-21]. Radiative heat transfer in squeezing flows also arises in magnetic recording technologies [22-25] where thin film non-Newtonian interfaces at the head-disk interface experience significantly high thermal loads. Several researchers have considered radiative squeezing flows of non-Newtonian lubricants. Mohyud-Din and Khan [26] presented homotopy solutions for unsteady dissipative squeezing flow of a viscoplastic fluid between an upper impermeable disk approaching a lower porous disk. They deployed a Rosseland diffusion flux model noting a significant elevation in temperature both in the core gap region and at the disk surfaces. A similar investigation was reported by Khan *et al*. [27] who also computed skin friction coefficient and local Nusselt number at both disks. Hayat *et al.* [28] computed the radiative squeezing flow of a magnetic second grade Reiner-Rivlin viscoelastic fluid with convective (Robin i.e. mixed) boundary conditions between approaching circular disks. They found that temperature is substantially elevated with radiation due to a reduction in mean absorption coefficient. They also showed that radial velocity exhibits a two different types of behavior by enlarging the magnetic parameter and that suction and injection modify both velocity and temperature distributions markedly. Heat transfer and entropy

generation on laminar natural convection of non-Newtonian nanofluids in the presence of an external horizontal magnetic field in a square cavity was analyzed by Kefayati [29]. Augmentation of the volume fraction and Rayleigh number enhanced all kinds of entropy generations of heat transfer, fluid friction, and the magnetic field. Bilal and Urva [30] studied the effects of nonlinear radiation and mixed convection for the Casson nanofluid through the thin needle. They claimed that the drag force over the fine needle was enhanced for the higher buoyancy ratio parameter and the rate of mass transfer was raised for the higher activation energy parameter.

As noted earlier, *heat dissipation and control* is a significant challenge in lubrication (squeezing) systems. Thermal management has therefore become a major focus in recent years in many industries where tribological systems feature e. g. aerospace, energy, heavy machinery, biomechanics, rail transit etc. An important development in this regard has been the introduction of *nanofluids* [31] instead of conventional fluids in the mid-1990s. Engineered at the nanoscale, nanofluids are colloidal suspensions of conventional base fluids e.g. lubricating oils doped with nanoscale metallic or carbon-based particles. Different types of nanofluids can be manufactured by suspending manually metals, carbides, oxides, nanotubes or nitrides of nano-size in the base fluid. The base fluids can be either Newtonian or non-Newtonian fluids and may be electrically non-conducting or magnetohydrodynamic fluids. In technical applications non-Newtonian fluids, as elaborated earlier, offer significant advantages over Newtonian fluids including superior oxidation inhibition, thermal dissipation, viscosity and decreased surfacial damage to bearing surfaces. Many elegant mathematical models have been developed for simulating nanofluid dynamics. Among the most popular is the two-component Buongiorno nanoscale model [32] which has the advantage of including a nanoparticle mass conservation (volume fraction) equation and also thermophoretic and Brownian dynamics effects. Although other approaches have been developed for nanoscale heat transfer [33], they are less compatible with viscous fluid dynamics analysis (e.g. squeezing hydrodynamics) and therefore Buongiorno's model remains very widely deployed since it permits the analysis of the nanoparticle concentration field (mass diffusion of nanoparticles). A number of works have been communicated in nanofluid squeezing flows in recent decades, motivated by the considerable thermal enhancement achieved by nanofluids without the agglomeration or clustering problems associated with larger (micron) sized particles. Hayat *et al.* [34] derived homotopy solutions for magnetohydrodynamic

squeezing flow of a Buongiorno nanofluid between parallel disks, observing that suction/injection at the walls noticeably alter velocity and temperature distributions and that increasing Brownian motion and thermophoresis parameters both elevate temperatures and nanoparticle concentrations.

Magnetohydrodynamic, non-Newtonian and other complex nanofluid flows have also been examined for other applications. Laminar mixed convection of non-Newtonian nanofluids in a square lid-driven cavity in the presence of a vertical magnetic field was analyzed by Kefayati [35]. It was found that the augmentation of Richardson number decreased heat transfer. Also the fall of the power law index declined heat transfer for different Richardson numbers. Hamid et al. [36] numerically analyzed the MHD flow of a nanofluid in converging/diverging channels through the Galerkin approach. The behavior of Prandtl numbers was increasing for temperature profile, while it was decreasing for concentration profile for both converging and diverging channels. Moreover, Lewis's number and Brownian motion parameter enhanced the concentration of fluid for both channels. The significance of velocity second slip model of non-Newtonian fluid on peristaltic pumping in existence of double-diffusivity convection in nanofluids and induced magnetic field was deliberated by Akram et al. [37]. They found that the pressure gradient was maximum in case of square wave. Further increase in stability of thermophoretic effects resulted in greater mass flux due to temperature rise which increased nanoparticles concentration. Aly and Mohamed [38] addressed the dispersion of the solid particles in nanofluid flow throughout the double-diffusive convection under the impacts of buoyancy ratio, magnetic field and three different boundary conditions. They showed that the variations on the boundary conditions of heat and mass differentiate dramatically the direction of solid particles dispersion in a cavity. Heat dissipation effect of a ferrofluid on natural convection flow in a cavity with linearly temperature distribution at the presence of an external magnetic source was studied by Kefayati [39]. It was found that the addition of the nanoscale ferromagnetic particle provoked the magnitude of velocity in the cavity to plummet noticeably. Heat transfer and entropy generation on laminar natural convection of non-Newtonian nanofluids in a porous square cavity was analyzed using Finite Difference Lattice Boltzmann Method by Kefayati [40]. It was found that the enhancement of the volume fraction augmented heat transfer and the entropy generations. Kefayati [41] studied laminar mixed convection of non-Newtonian nanofluids in a two sided lid-driven enclosure in the presence of a horizontal magnetic field.

Results drawn were that the augmentation of Richardson number decreased heat transfer. The addition of nanoparticle augmented heat transfer for a variety of parameters examined. Soomro et al. [42] examined the impact of Brownian motion and thermophoresis on MHD stagnation point nanofluid flow toward vertical stretching surface using the non-Newtonian Prandtl fluid model. Their study revealed that, in the buoyancy opposing flow region, the heat transfer rate increased, and the mass transfer rate decreased due to an increase in Brownian motion. Unsteady mixed convection flow and heat transfer of radiating and reacting nanofluid with variable transport properties in a microchannel filed with a saturated porous medium by taking into account the convective boundary conditions was researched by Rikitu et al. [43]. Both the heat transfer and the mass transfer rates at both sides of the microchannel walls were higher for large values of suction/injection Reynolds number, porous medium shape parameter and variable viscosity parameter. Afshar *et al.* [44] studied free convection of nanofluid as well as entropy generation inside a porous cavity loaded with nano-encapsulated phase change materials (NEPCMs). The results demonstrated that the various profiles of the wavy base section could affect the heat transmission features as well as fluid flow remarkably. Further it was also observed that all the profiles of entropy enhanced with increasing wave amplitude. The impact of non-dimensional fusion temperature on the free convection of conducting nanofluid within a porous enclosure filled with nano-encapsulated phase change materials (NEPCMs) was studied by Sattar *et al.* [45]. They concluded that the contribution of NEPCM enriched the heat transfer criterion due to improving thermal conductivity and heat capacity for the fusion temperature of the particles. They also found that higher Rayleigh number boosted average Nusselt number. The natural convection of a magnetohydrodynamic nanofluid in an enclosure under the effects of thermal radiation and the shape factor of nanoparticles was analyzed numerically using the control-volume-based finite element method by Chamkha *et al.* [46]. Their findings demonstrated that the laminate-shaped nanoparticles have a more notable impact on the average and local Nusselt numbers than other nanoparticle shapes. Magnetic nanofluid natural convection in the porous enclosure considering Brownian motion was studied by Dogonchi *et al.* [47] numerically using Control Volume Finite Element Method. Their results indicated that the intensity of the convective flow has a direct relationship with the Rayleigh number and Darcy number while it has a reverse relationship with the Hartmann number and inclination angle of the magnetic field. The incremental impact of nonlinear thermal radiation on heat transfer

enhancement due to Darcy–Forchheimer flow in $MnFe_2O_4$-Casson/water nanofluids from a stretched rotating disk was researched by Sachin *et al.* [48]. They claimed that an increase in thermal radiation boosted the heat propagating into the fluid leading to a thicker thermal boundary layer. Fluids with non-Newtonian behavior were shown to produce higher entropy generation rates compared to Newtonian fluids. Entropy generation in a nanofluid-filled semi-annulus cavity with nanoparticle shape effects was investigated by Seyyed *et al.* [49]. Their results showed that the Nusselt number and entropy generation number are escalated by increasing the Rayleigh number and the nanoparticle volume fraction.

More recently, several other interesting studies of magnetic nanofluid squeezing heat transfer have been communicated. Saidi *et al.* [50] used Runge-Kutta quadrature to compute the radial, tangential and axial velocities, pressure gradient, temperature and concentration distributions for transient hydromagnetic squeezing flow of a nanofluid with the Buongiorno model. Ahmed *et al.* [51] used Hamilton-Crosser and Brinkman nanoscale models with Adomian decomposition, variation of parameter (VPM) and Runge-Kutta quadrature to examine nanoparticle shape factor effects (for bricks, platelets and cylinder geometries) in transient squeezing flow of magneto-nanofluid between two parallel disks with viscous heating. They observed that a sharper temperature elevation is computed for brick shaped nanoparticles. Other studies on nanofluid squeezing include Das *et al.* [52] (who included slip effects), Bég *et al.* [53] (who used a B-spline collocation method to verify the homotopy solutions of Hayat *et al.* [34] and also computed torques at the upper and lower disks), Sobamowo and Akinshilo [54] (who used a Tiwari-Das nanoscale model to study hydromagnetic squeezing flow of Cu-water and Cu kerosene nanofluids with a regular perturbation method). Thermal radiation effects on reactive magnetic nanofluid squeezing flow were explored by Ullah *et al.* [55] who showed that temperatures are augmented with both stronger radiative heat flux and Brownian diffusion effects.

In the present work, motivated by simulating the high temperature squeezing behavior of nano-doped magnetorheological plastomers (MRPs) [12], a mathematical model is derived for *radiative squeezing flow of magnetohydrodynamic viscoplastic nanofluid between coaxial circular disks*. This problem has thus far not received the attention of the scientific community. MRPs are known to achieve a higher yield stress under squeeze flow than conventional

magnetorheological fluids and when further modified with nanoparticles are expected to hold significant promise in thermal management in lubrication systems. The Buongiorno nanoscale model and the Casson yield stress rheological model are used. The Casson model has been very popular in lubrication rheological studies as it quite accurately simulates actual viscoplastic lubricants [56-59] and is relatively simple mathematically. To generalize the thermal analysis, *Fourier* boundary conditions are implemented at the disks. Also known as *Robin* boundary conditions or convective boundary conditions in heat transfer [60, 61], they are a weighted combination of Dirichlet boundary conditions and Neumann boundary conditions and allow for a more complex characterization of squeezing transport phenomena. The conservation equations are reduced to ordinary differential equations with the aid of similarity transformations. A 4th order Runge-Kutta solver (MATLAB bvp4c) [62] is deployed to obtain numerical solutions for the emerging nonlinear, coupled ordinary differential boundary value problem. Verification of solutions for special cases in the literature is included. Extensive visualization of the impact of key rheological, nanoscale, magnetic and thermophysical parameters on transport characteristics (velocity, temperature, nanoparticle concentration etc) are provided.

2. Thermo-magnetic rheological nanofluid squeezing flow model

The physical domain (see **Fig. 1**) of interest comprises the unsteady squeezing flow of an electrically conducting viscoplastic (Casson) nanofluid between two parallel disks. Unidirectional (axial) thermal radiative flux is included as is viscous heating. The distance between disks is $h(t) = H(1-at)^{1/2}$. A magnetic field is applied perpendicular to the plane of the disks (i.e. axially) and has strength $B(t) = B_0(1-at)^{-1/2}$. Edge effects at the disks are ignored as is surface roughness i. e. the disks are smooth. The lower porous disk is situated at $z = 0$ which is stationary (suction or injection are present) and the upper impervious disk is positioned at $z = h(t)$ and is moving with the velocity $aH(1-at)^{-1/2}/2$ towards the lower disk. Hall current and magnetic induction effects are ignored. (T_w, T_h) and (C_w, C_h) denote the temperatures and nanoparticle concentrations at the lower disk and upper disk respectively. Rosseland's diffusion flux approximation is implemented for radiative transfer and is valid for optically thick lubricants.

Under these approximations, the conservation equations for the regime may be presented following Hayat *et al.* [63] and Hashmi *et al*. [64] as:

$$\frac{\partial u}{\partial r}+\frac{u}{r}+\frac{\partial w}{\partial Z}=0, \tag{1}$$

$$\frac{\partial u}{\partial t}+u\frac{\partial u}{\partial r}+w\frac{\partial u}{\partial z}=\frac{-1}{\rho}\frac{\partial P}{\partial r}+\upsilon\left[\frac{1+\beta}{\beta}\right]\left[\frac{\partial^2 u}{\partial r^2}+\frac{\partial^2 u}{\partial z^2}+\frac{1}{r}\frac{\partial u}{\partial r}-\frac{u}{r^2}\right]-\frac{\sigma}{\rho}B^2(t)u, \tag{2}$$

$$\frac{\partial w}{\partial t}+u\frac{\partial w}{\partial r}+w\frac{\partial w}{\partial z}=\frac{-1}{\rho}\frac{\partial P}{\partial z}+\upsilon\left[\frac{1+\beta}{\beta}\right]\left[\frac{\partial^2 w}{\partial r^2}+\frac{\partial^2 w}{\partial z^2}+\frac{1}{r}\frac{\partial w}{\partial r}\right], \tag{3}$$

$$\begin{aligned}\frac{\partial T}{\partial t}+u\frac{\partial T}{\partial r}+w\frac{\partial T}{\partial z}=\alpha\left[\frac{\partial^2 T}{\partial r^2}+\frac{1}{r}\frac{\partial T}{\partial r}+\frac{\partial^2 T}{\partial z^2}\right]+\tau\left[D_B\left(\frac{\partial C}{\partial r}\frac{\partial T}{\partial r}+\frac{\partial C}{\partial z}\frac{\partial T}{\partial z}\right)+\frac{D_T}{T_m}\left(\left(\frac{\partial T}{\partial r}\right)^2+\left(\frac{\partial T}{\partial z}\right)^2\right)\right]\\ +\frac{\upsilon}{C_P}\left[2\frac{u^2}{r^2}+\left(\frac{\partial u}{\partial r}\right)^2+2\left(\frac{\partial w}{\partial z}\right)^2+2\left(\frac{\partial u}{\partial r}\right)^2+2\left(\frac{\partial w}{\partial r}\right)^2+2\frac{\partial u}{\partial z}\frac{\partial w}{\partial r}\right]-\frac{1}{\rho C_P}\frac{\partial q_r}{\partial z},\end{aligned} \tag{4}$$

$$\frac{\partial C}{\partial t}+u\frac{\partial C}{\partial r}+w\frac{\partial C}{\partial z}=D_B\left[\frac{\partial^2 C}{\partial r^2}+\frac{1}{r}\frac{\partial C}{\partial r}+\frac{\partial^2 C}{\partial z^2}\right]+\frac{D_T}{T_m}\left[\frac{\partial^2 T}{\partial r^2}+\frac{1}{r}\frac{\partial T}{\partial r}+\frac{\partial^2 T}{\partial z^2}\right]. \tag{5}$$

The upper disk and the lower disk boundary conditions are prescribed respectively as:

$$u=0, w=\frac{dh}{dt}, -k\frac{\partial T}{\partial z}\bigg|_{z=h(t)}=h_2\left[T\left(r,z(t)\right)-T_h\right],\ C=C_h \quad \text{at } z=h(t), \tag{6}$$

$$u=0,\ w=\frac{-w_0}{\sqrt{1-at}}, -k\frac{\partial T}{\partial z}\bigg|_{z=0}=h_1\left[T_w-T(r,0)\right],\ C=C_w \quad \text{at } z=0. \tag{7}$$

The notations used in the above equations are as follows: density (ρ); pressure $(\tilde{p})$; dynamic viscosity (υ); Casson parameter $\left(\beta=\mu_B\sqrt{\frac{2\pi_c}{p_y}}\right)$, π_c is the critical value of π; specific heat (C_P); thermal diffusivity (α); thermal diffusion coefficient (D_T); Brownian motion coefficient D_B, radiative heat flux (q_r); thermal conductivity (k); mean fluid temperature (T_m), velocity along r direction (u); velocity along (z) direction; temperature (T);

concentration (C); suction/injection velocity (w_0); ratio of heat capacity of the nanoparticles to the heat capacity of the fluid (τ); thermophoretic diffusion coefficient (D_B) and Brownian motion coefficient (D_B). Further details of the Casson model are given in the Appendix.

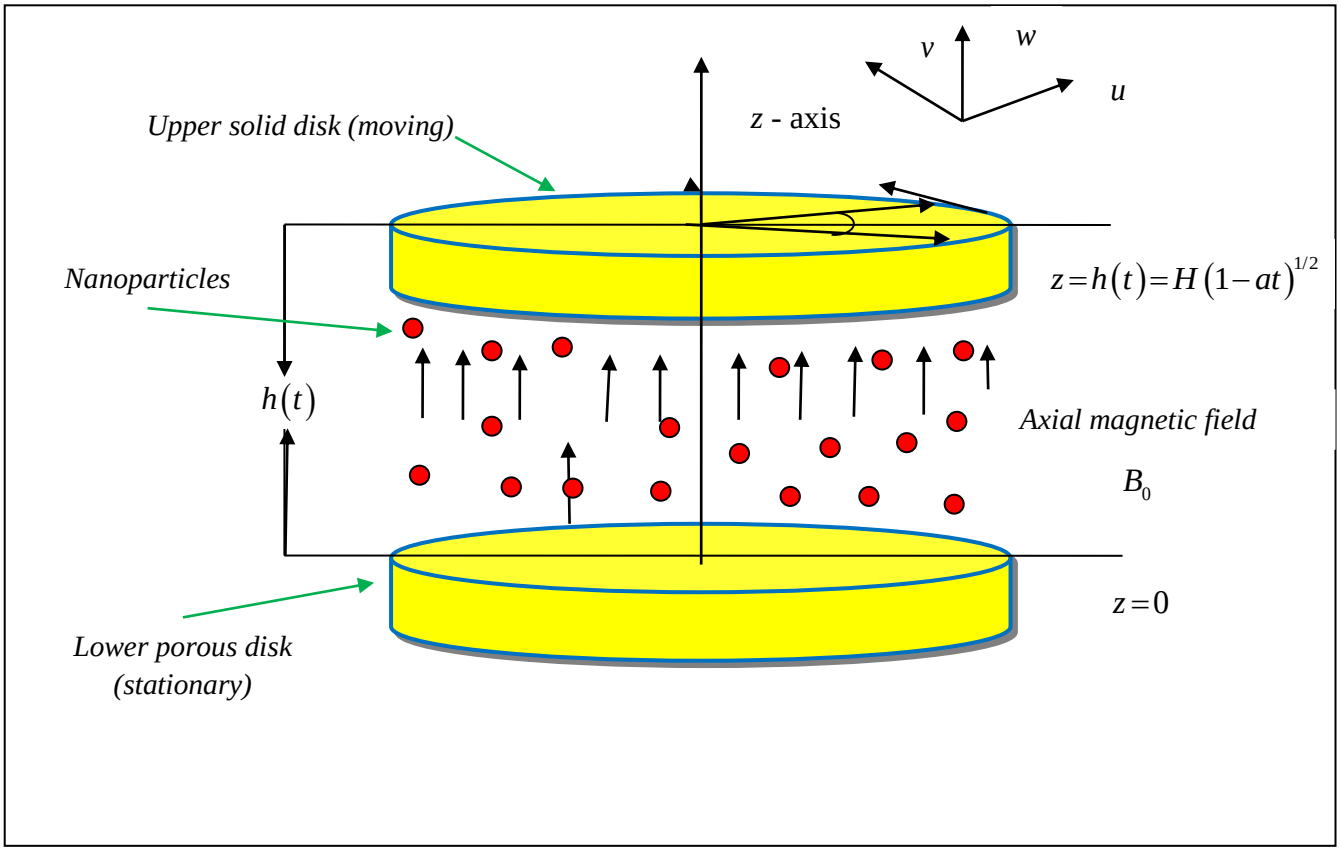

Figure 1 Physical representation of the problem

The radiative heat flux q_r is (for details see Modest [63]) analyzed with the Rosseland model:

$$q_r = \frac{-4\sigma^*}{3k^*}\frac{\partial\left(T^4\right)}{\partial z} \tag{8}$$

The coefficient of mean absorption is k^* and the Stefan-Boltzmann constant is σ^*. Considering

$$T^4 \cong -3T_h^4 + 4T_h^3 T\,, \tag{9}$$

It follows from Eqn. (8) that:

$$\frac{\partial q_r}{\partial z} = \frac{-16\sigma^* T_h^3}{3k^*}\frac{\partial^2 T}{\partial z^2}\ . \tag{10}$$

Equation (10) after including Eq. [10] become

$$\begin{aligned}\frac{\partial T}{\partial t} + u\frac{\partial T}{\partial r} + w\frac{\partial T}{\partial z} = \alpha\left[\frac{\partial^2 T}{\partial r^2} + \frac{1}{r}\frac{\partial T}{\partial r} + \frac{\partial^2 T}{\partial z^2}\right] + \tau\left[D_B\left(\frac{\partial C}{\partial r}\frac{\partial T}{\partial r} + \frac{\partial C}{\partial z}\frac{\partial T}{\partial z}\right) + \frac{D_T}{T_m}\left(\left(\frac{\partial T}{\partial r}\right)^2 + \left(\frac{\partial T}{\partial z}\right)^2\right)\right] \\ + \frac{\upsilon}{C_P}\left[2\frac{u^2}{r^2} + \left(\frac{\partial u}{\partial r}\right)^2 + 2\left(\frac{\partial w}{\partial z}\right)^2 + 2\left(\frac{\partial u}{\partial r}\right)^2 + 2\left(\frac{\partial w}{\partial r}\right)^2 + 2\frac{\partial u}{\partial z}\frac{\partial w}{\partial r}\right] - \frac{1}{\rho C_P}\frac{16\sigma^* T_\infty^3 \partial^2 T}{3k^* H^2 \partial z^2}.\end{aligned} \tag{11}$$

For the purpose of non-dimensionalization, following group of similarity transformation are defined

$$\begin{aligned} u &= \frac{a r}{2(1-a t)} f^1(\eta),\ \ w = \frac{-a H}{\sqrt{1-a t}} f(\eta),\ \eta = \frac{z}{H\sqrt{1-a t}}, \\ B(t) &= \frac{B_0}{\sqrt{1-a t}},\ \theta = \frac{T-T_h}{T_w - T_h},\ \ \phi = \frac{C-C_h}{C_w - C_h} \end{aligned} \tag{12}$$

Insertion of Eqn. (12) in Eqns. (1) to (5) (after eliminating pressure gradient) yields the following trio of momentum, energy and nanoparticle species conservation ordinary differential equations:

$$\left(\frac{1+\beta}{\beta}\right) f'''' - S\left(\eta f''' + 3f'' - 2ff'''\right) - M^2 f'' = 0, \tag{13}$$

$$\begin{aligned}\left(1+\frac{4}{3}Rd\right)\theta'' + \Pr S\left(2f\theta' - \eta\theta'\right) + \Pr\left(Nb\,\theta'\phi' + Nt\,\theta'^2\right) \\ + \Pr Ec\left(12\delta^2 f'^2 + f''^2\right) = 0,\end{aligned} \tag{14}$$

$$\phi'' + LeS\left(2f\phi' - \eta\phi'\right) + \frac{Nt}{Nb}\theta'' = 0, \tag{15}$$

The transformed boundary conditions at the *lower and upper disks* are:

$$f(0) = A,\ f'(0) = 0,\ \theta'(0) = Bi_1\left[\theta(0) - 1\right],\ \phi(0) = 1 \qquad \text{at } \eta = 0, \tag{16}$$

$$f(1) = \frac{1}{2},\ f'(1) = 0,\ \theta'(1) = Bi_2\left[\theta(1)\right],\ \phi(1) = 0 \qquad \text{at } \eta = 1, \tag{17}$$

Here $S = \frac{a H^2}{2\upsilon}$ (squeezing number); $A = \frac{w_0}{a H}$ (suction/injection parameter at the lower disk); $M = \sqrt{\frac{\sigma B_0^2 H^2}{\upsilon}}$ (Hartmann magnetic body force number); $Ec = \frac{1}{C_P (T_w - T_h)} \left(\frac{a r}{2(1-at)} \right)^2$ (Eckert viscous heating number); $\Pr = \frac{\upsilon}{\alpha}$ (Prandtl number); $Le = \frac{\upsilon}{D_e}$ (Lewis number); $Rd = \frac{4\sigma^* T_h^3}{k k^*}$ (radiation parameter); $\delta^2 = \frac{H^2 (1-at)}{r^2}$ (dimensionless length parameter); $Nt = \frac{(\rho C)_p D_T (T_w - T_h)}{(\rho C)_f T_m \upsilon}$ (thermophoresis parameter); and $Nb = \frac{(\rho C)_p D_B (C_w - C_h)}{(\rho C)_f \upsilon}$ (Brownian motion parameter).

The positive values of A denote *suction* and negative values denotes *injection* of the viscoplastic nanofluid from or into the lower disk. The case $A = 0$ implies that the lower disk is solid.

The skin friction coefficient (C_{fr}) i.e. dimensionless surface shear stress, the Nusselt number (Nur) i.e. dimensionless wall heat transfer rate, and the Sherwood number (Shr) i.e. dimensionless nanoparticle species transfer rate, at a disk surface are defined as:

$$C_{fr} = \frac{\tau_{rz}\big|_{z=h(t)}}{\rho \left(\frac{-aH}{2(1-at)^{1/2}} \right)^2}, \; Nur = \frac{H q_w}{k (T_w - T_h)}, \; Shr = \frac{H j_w}{D_B (C_w - C_h)}, \tag{18}$$

$$\text{where, } \tau_{rz} = \mu \left(\frac{\partial u}{\partial z} + \frac{\partial w}{\partial r} \right)\Bigg|_{z=h(t)}, \; q_w = -k \left(\frac{\partial T}{\partial z} \right)\Bigg|_{z=h(t)}, \; j_w = -D_B \left(\frac{\partial C}{\partial z} \right)\Bigg|_{z=h(t)}. \tag{19}$$

In terms of the variables in Eqns. (6) and (7), we get:

$$\frac{H^2}{r^2} \mathrm{Re}_r C_{fr} = f''(1), \quad Nur = (1-at)^{1/2} Nu = -\theta'(1), \; Shr = (1-at)^{1/2} Sh = -\phi'(1) \tag{20}$$

Here $\mathrm{Re}_r = \frac{r a H (1-at)^{1/2}}{2\upsilon}$ is a squeezing Reynolds number.

3. Numerical Solutions with MATLAB bvp4c and Validation

The ordinary differential boundary value problem defined by Eqns. (13)-(15) with boundary conditions (16, 17) is highly nonlinear and analytical solutions are intractable. Moreover, the presence of boundary conditions of the Fourier type renders the boundary value problem more complicated. A computational solution is therefore sought. A MATLAB routine based on a numerical method bvp4c is deployed. Extensive details of this solver are given in Kierzenka and Shampine [43]. Many engineering problems have been successfully solved by this method. **Table 1** details the comparison of the results obtained by MATLAB bvp4c with the homotopy solutions of Hashmi *et al.* [34]. The comparison is made considering the absence of nanoparticles, radiation and length effects in the present model. The skin friction values are equal up to four decimal places and hence the present MATLAB code is verified for accuracy.

Table 1 Comparison table for Skin friction coefficient $f''(1)$ for different values of M and S for $A = 2,\ P = Le = 1,\ Nt = Nb = 0.1,\ \beta = 0, \delta = 0,\ Ec = 0$

M	S	$f''(1)$		
		Present $Bi_1 = Bi_2 = 10$	Present $Bi_1 = 1.0,\ Bi_2 = 10$	Hashmi et al [34]
0	1	7.53313247	7.53313247	7.53316579
2	1	8.26383886	8.26384197	8.26387231
3	1	9.09725938	9.09726618	9.09732572
5	1	11.3492988	11.3493158	11.3492890
1	0.1	8.97546290	8.97546290	8.97552394
1	0.5	8.34917873	8.34916801	8.34924578
1	1	7.72190940	7.72191376	7.72194601
1	2	6.94081636	6.94082584	6.94077326

4. Results and Discussion

Figs. 2-9 illustrate the MATLAB bvp4c results obtained for velocity, temperature and nanoparticle concentration with various parameters. Figures 2a and 2b display the impact of

squeezing parameter, S for both suction and blowing (A) on the velocity, temperature and nanoparticle species concentration profiles for identical Biot numbers at the disks $(Bi_1 = Bi_2)$ and unequal Biot numbers at the disks $(Bi_1 \neq Bi_2)$. As noted earlier for suction $(A > 0)$ and for blowing i.e. lateral mass flux into the lower disk $(A < 0)$. The velocity is reduced near the disk surfaces (η=*0 at the lower disk and* η *= 1 at the upper disk*) up to $\eta \leq 4$ in the gap region, and then raises as S expands. These figures also reveal that the velocity contours for suction are opposite to the injection for all values of Bi.

The effect of magnetic number, M on the flow is plotted in Figures 3a and 3b. The velocity (radial) grows near the disks; while in the center, it declines for $Bi_1 = Bi_2$ and $Bi_1 \neq Bi_2$. Further one can also conclude that the influence of M is more predominant at the upper disk relative to the lower disk.

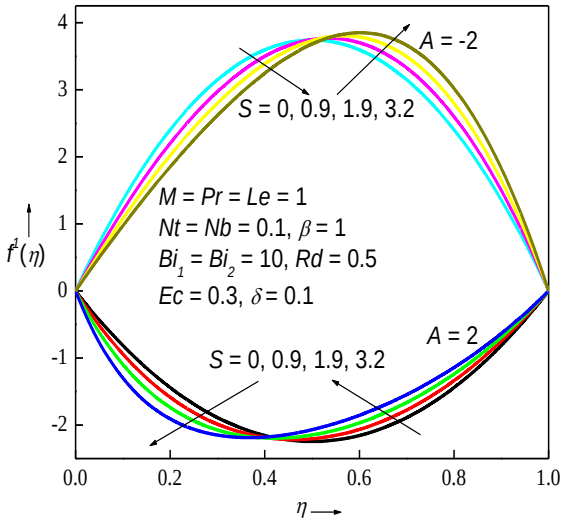

Figure 2a Influence of S on $f'(\eta)$ for equal Biot numbers.

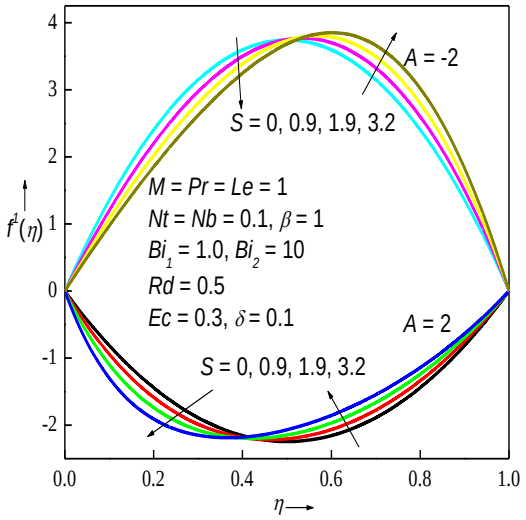

Figure 2b Influence of S on $f'(\eta)$ for unequal Biot numbers.

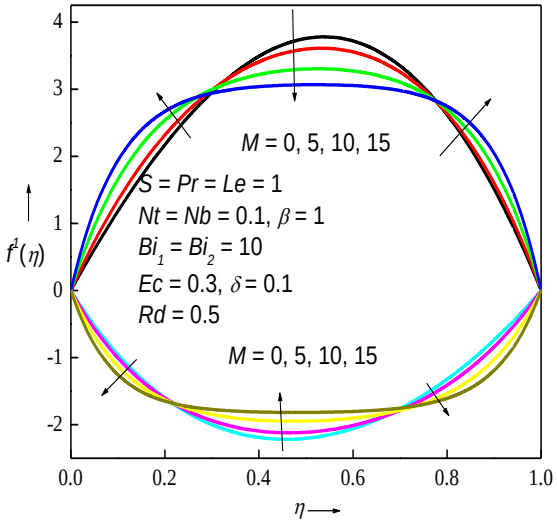

Figure 3a Influence of M on $f'(\eta)$ for equal Biot numbers.

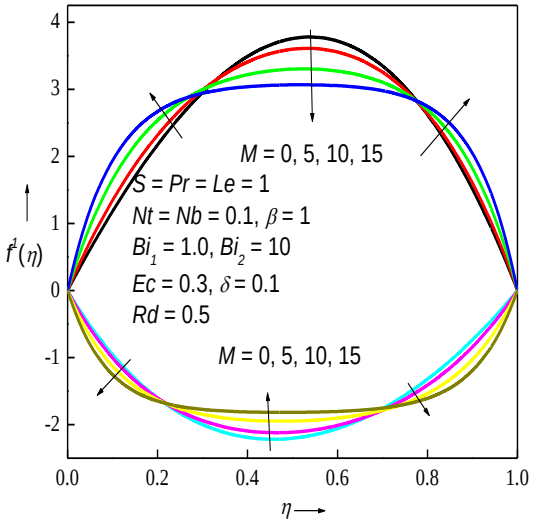

Figure 3b Influence of M on $f'(\eta)$ for unequal Biot numbers.

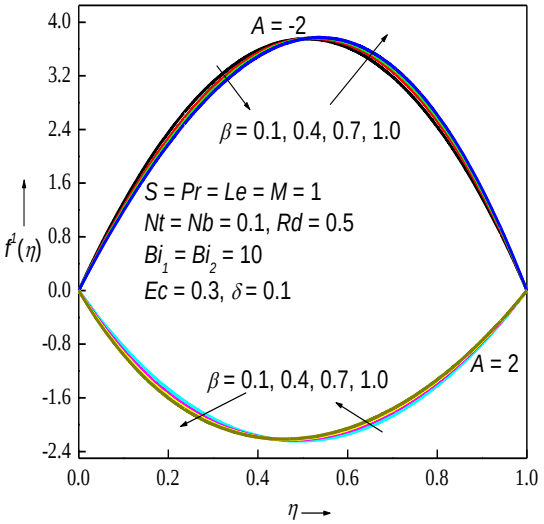

Figure 4a Influence of β on $f'(\eta)$ for equal Biot numbers.

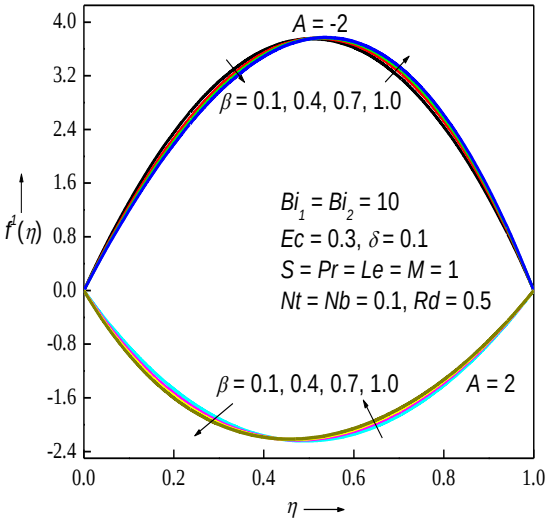

Figure 4b Influence of β on $f'(\eta)$ for unequal Biot numbers.

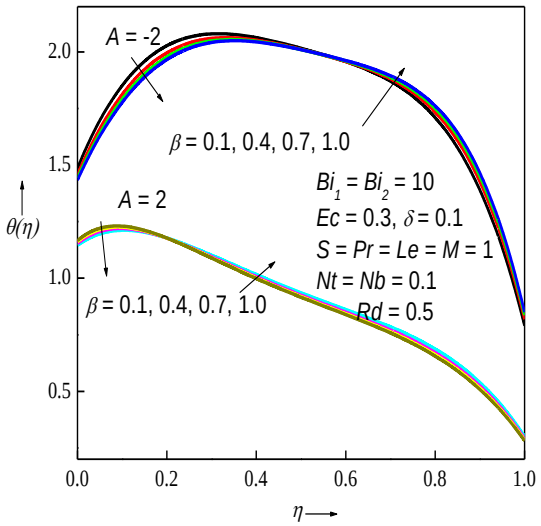

Figure 4c Influence of β on $\theta(\eta)$ for equal Biot numbers.

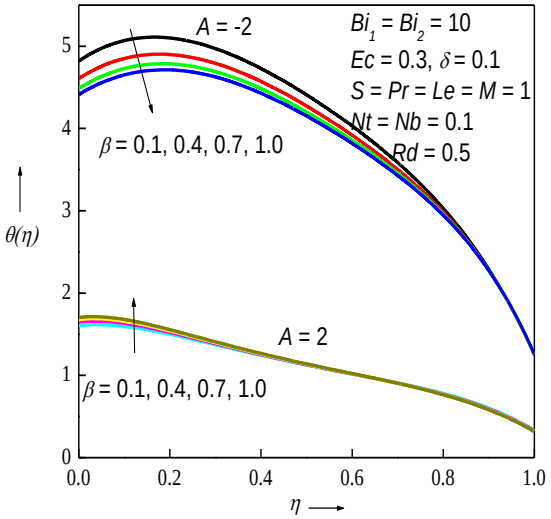

Figure 4d Influence of β on $\theta(\eta)$ for unequal Biot numbers.

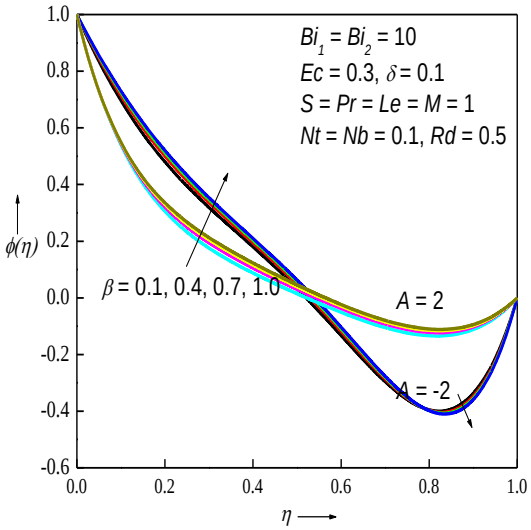

Figure 4e Influence of β on $\phi(\eta)$ for equal Biot numbers.

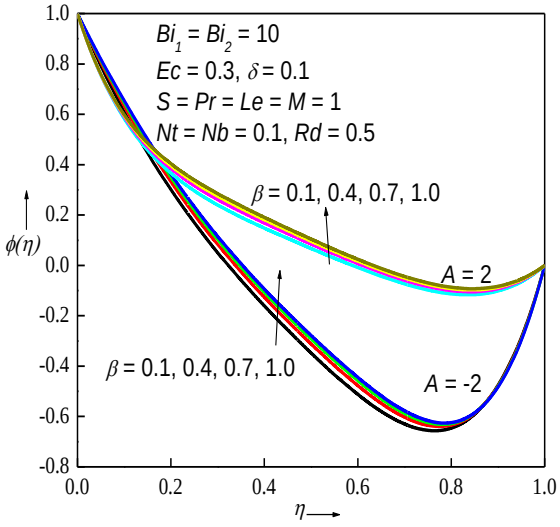

Figure 4f Influence of β on $\phi(\eta)$ for unequal Biot numbers.

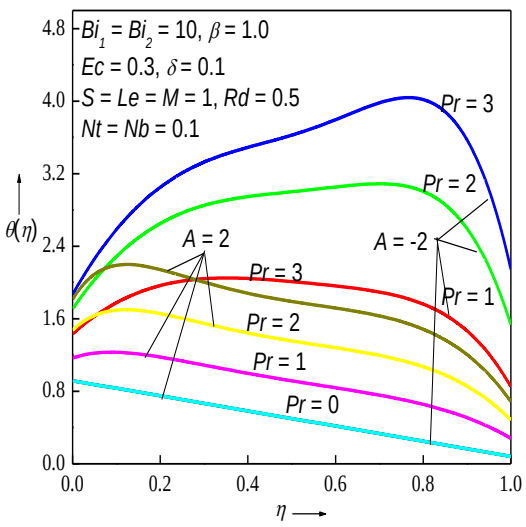

Figure 5a Influence of *Pr* on $\theta(\eta)$ for equal Biot numbers.

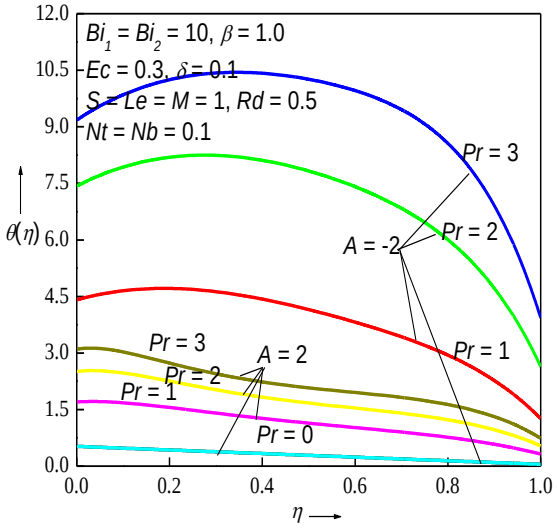

Figure 5b Influence of *Pr* on $\theta(\eta)$ for unequal Biot numbers.

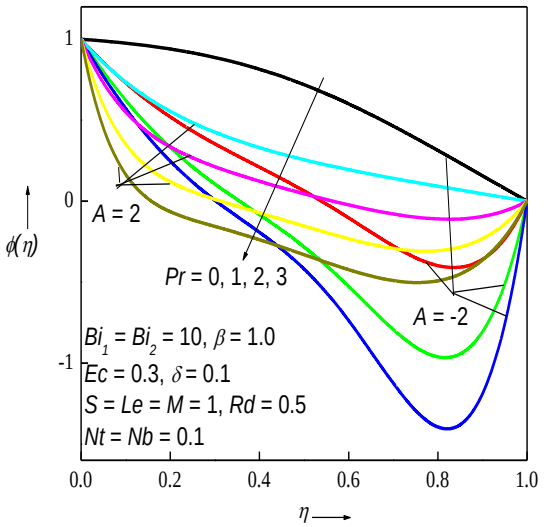

Figure 5c Influence of *Pr* on $\phi(\eta)$ for equal Biot numbers.

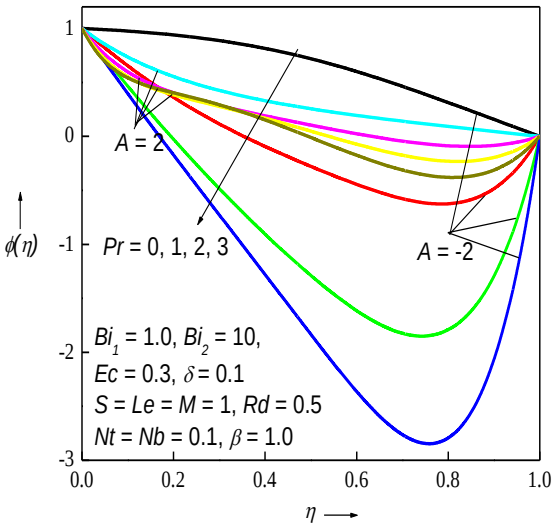

Figure 5d Influence of *Pr* on $\phi(\eta)$ for unequal Biot numbers.

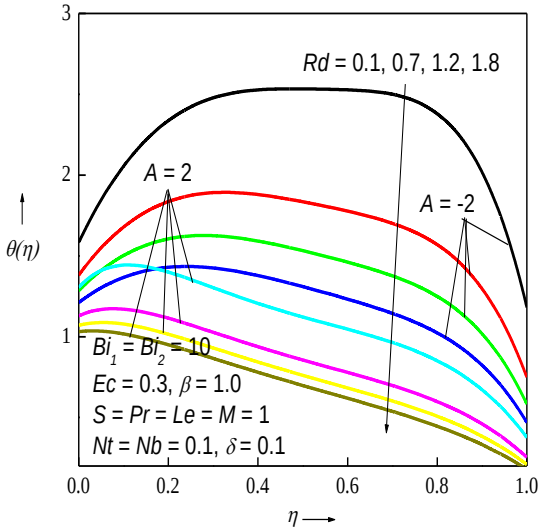

Figure 6a Influence of *Rd* on $\theta(\eta)$ for equal Biot numbers.

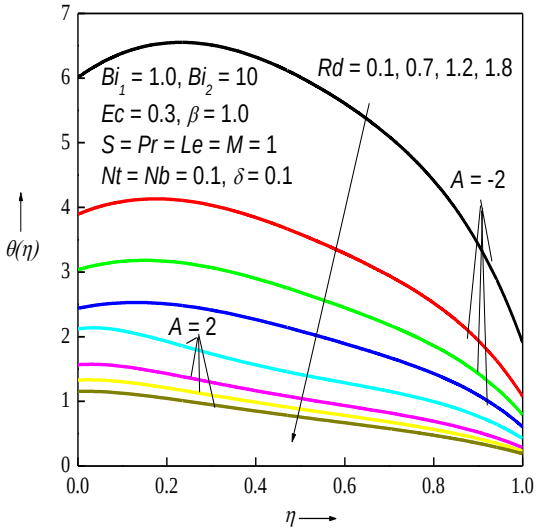

Figure 6b Influence of *Rd* on $\theta(\eta)$ for unequal Biot numbers.

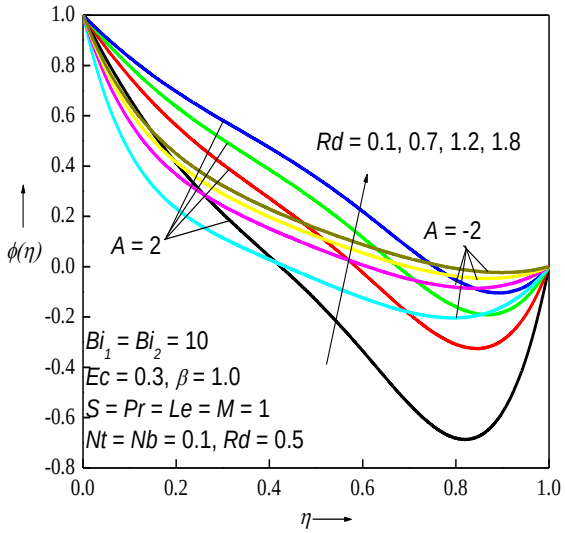

Figure 6c Influence of *Rd* on $\phi(\eta)$ for equal Biot numbers.

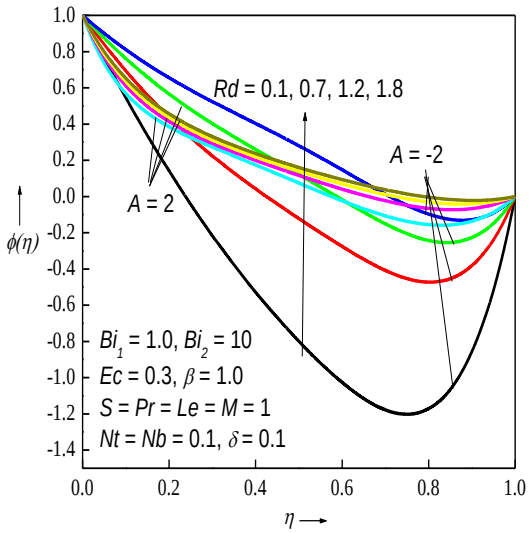

Figure 6d Influence of *Rd* on $\phi(\eta)$ for unequal Biot numbers.

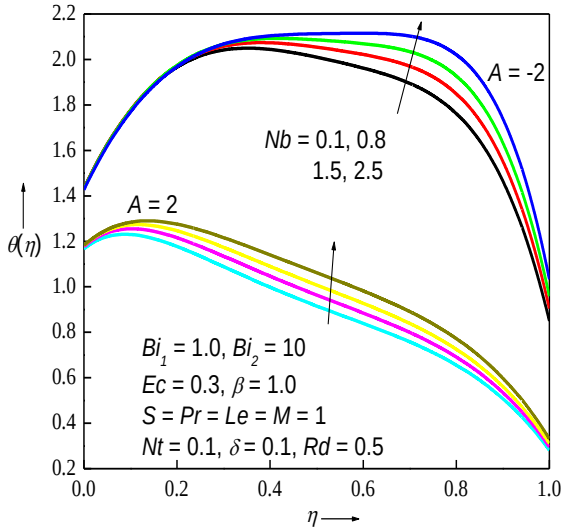

Figure 7a Influence of *Nb* on $\theta(\eta)$ for equal Biot numbers.

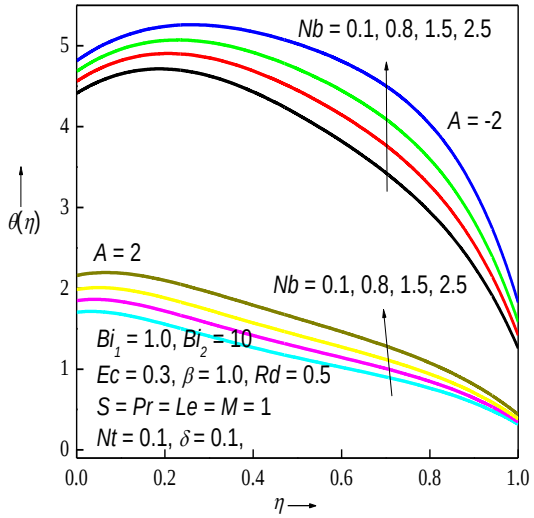

Figure 7b Influence of *Nb* on $\theta(\eta)$ for unequal Biot numbers.

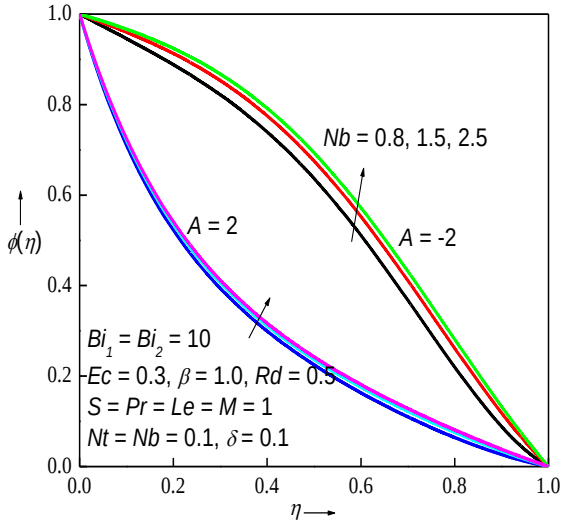

Figure 7c Influence of *Nb* on $\phi(\eta)$ for equal Biot numbers.

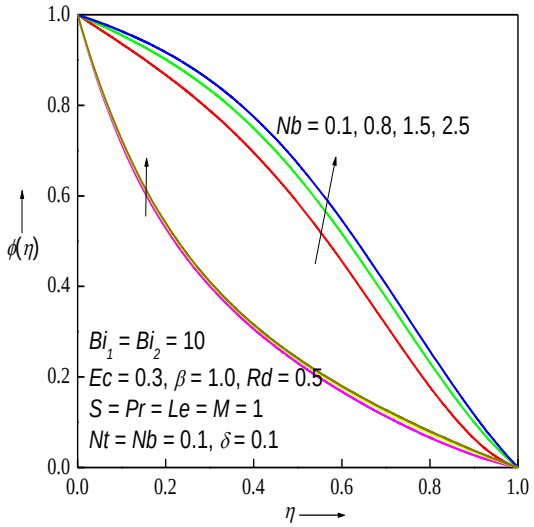

Figure 7d Influence of *Nb* on $\phi(\eta)$ for unequal Biot numbers.

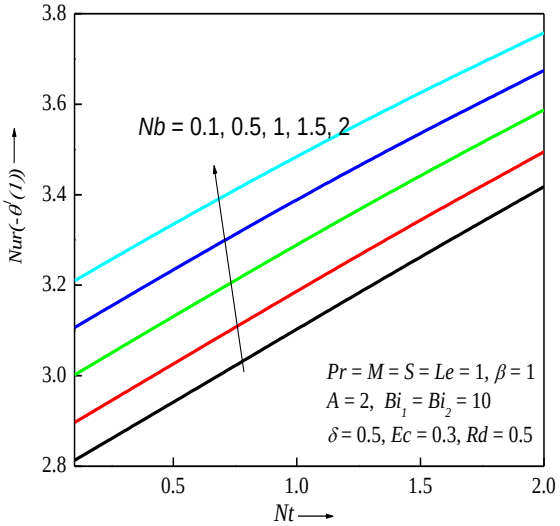

Figure 8a Influence of *Nb* and *Nt* on *Nur* for equal Biot numbers.

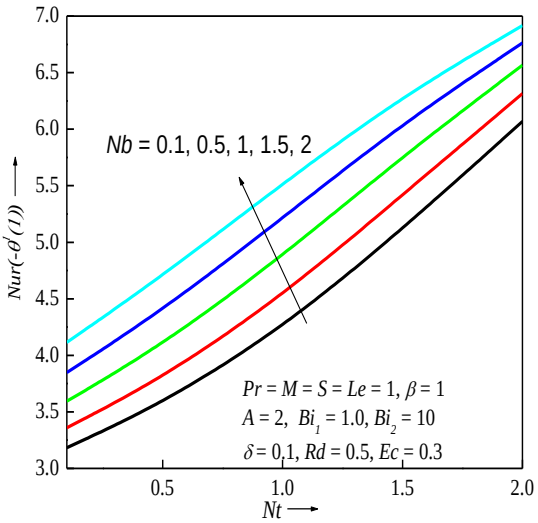

Figure 8b Influence of *Nb* and *Nt* on *Nur* for unequal Biot numbers.

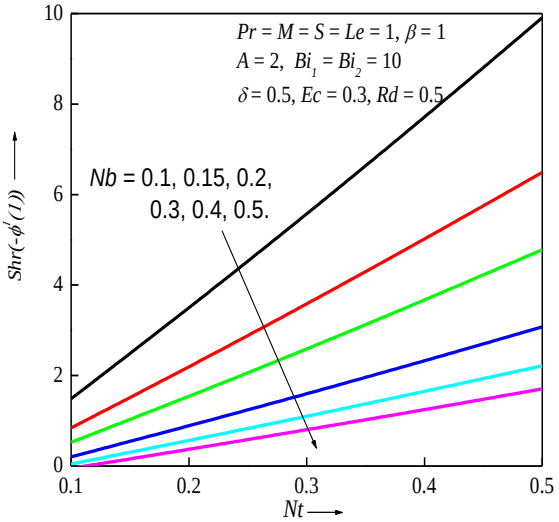

Figure 9a Influence of *Nb* and *Nt* on *Shr* for equal Biot numbers.

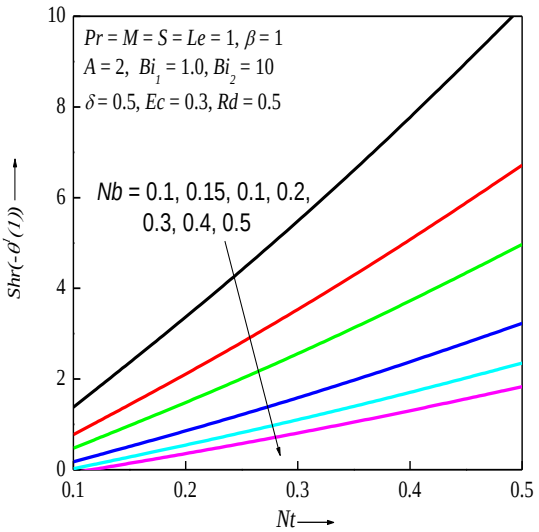

Figure 9b Influence of *Nb* and *Nt* on *Shr* for unequal Biot numbers.

Table 2 Effect of β on temperature with

$A = 2, S = M = P = Le = 1, Nb = Nt = 0.1, Ec = 0.3, \delta = 0.1, Rd = 0.5.$

	$\theta(\eta)$					
	$Bi_1 = Bi_2 = 10$			$Bi_1 = 1.0, Bi_2 = 10$		
η	$\beta = 0$	$\beta = 1$	$\beta = 10$	$\beta = 0$	$\beta = 1$	$\beta = 10$
0	1.14096439	1.167061275	1.19679198	1.587959079	1.703060238	1.83434617
0.2	1.183723126	1.18388357	1.19316294	1.50090673	1.56691012	1.65134262
0.4	1.026995808	1.00340585	0.99656619	1.25003687	1.27459025	1.32266608
0.6	0.870956750	0.84205266	0.82873223	1.02266771	1.02731770	1.05230052
0.8	0.698094688	0.65826276	0.63517532	0.78825841	0.76862122	0.76857930
1.0	0.306086132	0.28129480	0.26663594	0.33635413	0.31834096	0.31142719

Table 3 Effect of different values of β on Nusselt number, skin friction coefficient and Sherwood number for $A = 2, S = M = P = Le = 1, Nb = Nt = 0.1, Ec = 0.3, \delta = 0.1, Rd = 0.5.$

	$f''(1)$		$-\theta'(1)$		$-\phi'(1)$	
β	$Bi_1 = Bi_2 = 10$	$Bi_1 = 1.0,$ $Bi_2 = 10$	$Bi_1 = Bi_2 = 10$	$Bi_1 = 1.0,$ $Bi_2 = 10$	$Bi_1 = Bi_2 = 10$	$Bi_1 = 1.0,$ $Bi_2 = 10$
0.1	8.85128394	8.85128660	-3.0097824	-3.32265546	1.73993148	1.64367188
0.5	8.48672784	8.48674643	-2.8867398	-3.23135726	1.58239175	1.47989364
1.0	8.26328333	8.26328684	-2.8129480	-3.18340964	1.48457414	1.37701069
5.0	7.88154991	7.88154964	-2.6900187	-3.12208903	1.31276067	1.19350542
10	7.80650070	7.80650155	-2.6663594	-3.11427189	1.27787314	1.15571216

Figures 4a and 4b, depict the response of Casson parameter β on the velocity for any values of Bi and for injection and suction conditions. This parameter augments the shear term in the transformed momentum Eqn. (13), $\left(\frac{1+\beta}{\beta}\right) f'''$.When $A<0$, in the injection case, the velocity decreases up to $\eta = 0.5$ and then increases; a similar trend is noticed in suction case up to $\eta = 0.4$. In Figures 4c, d and 4e, the influence of Casson viscoplastic parameter, β on the heat and nanoparticle concentration fields are presented. In Figures 4c and 4d it is seen that the impact of β is more pronounced on temperatures at the lower (porous) disk than that at the upper (solid) disk. There is a weaker elevation in nanoparticle concentration field as shown in Figures 4e and 4f when compared with the temperature field.

The effects of the Pr on temperature, θ are captured in **Figures 5a and 5b** for $Bi_1 = Bi_2$ and $Bi_1 \neq Bi_2$. There is a speedy growth in θ as Pr is accentuated owing to the addition of viscous dissipation effects. For liquid-like materials which have the property of low viscosity and high thermal conductivity, there will be correspondingly smaller values of Pr. Large values of Pr represent higher viscosity liquids e.g. lubricants, oils, greases etc. The effect of the Prandtl number Pr on the nanoparticle concentration profiles is depicted in **Figures 5c and 5d** for identical and distinct Bi. The reverse trend is observed with a change in Prandtl number, in nanoparticle concentration, ϕ relative to the temperature field, θ. In other words as Pr is inflated, ϕ depletes and its influence is diminished at the lower disk when matched with the upper disk for $A>0$ and vice versa for $A<0$. Analogous results are seen for the effects of Eckert number, Ec and length parameter, δ on u, θ and ϕ as with Pr and hence not presented. The effects of radiative parameter, Rd on θ and ϕ are depicted in **Figures 6a to 6d**. Upgrading the values of Rd, which correspond to stronger thermal conduction and weaker radiative flux, reduce θ; however they increase nanoparticle concentration magnitudes, ϕ for both equal and unequal Biot numbers Bi at the two disks. The influence of Rd is more effective at the lower disk than at the upper disk on the temperature field θ and the opposite behavior is computed for nanoparticle concentration, ϕ.

Figures 7a-7d illustrate the influence of Brownian motion parameter, Nb on θ and ϕ for $Bi_1 = Bi_2$ and $Bi_1 \neq Bi_2$. The larger values of Nb (which correspond to physically smaller

sized nanoparticles in the Buongiorno model [28]) is to elevate magnitudes of both θ and ϕ for any values of Bi. However the response is more prominent for $A=-2$ (injection at lower disk) when compared to $A=2$ (suction at the lower disk) for both θ and ϕ. Similar results are obtained for the influence of thermophoresis parameter, Nt and therefore not presented.

The combined influence of Nb and Nt on Nur and Shr for $Bi_1 = Bi_2$ and $Bi_1 \neq Bi_2$ are depicted in **Figs. 8a, b and 9a, b** respectively. The Nusselt number values Nur are considerably enhanced with an increment in Nb and Nt (Figs 8a,b) whereas and the Sherwood values are depressed by enlarging Nb but increased with greater Nt (Figs. 9a,b). Heat transfer to the disk surfaces is therefore intensified with stronger Brownian motion and thermophoretic body force effects whereas nanoparticle mass transfer to the disk surfaces is depleted with stronger Brownian motion but enhanced with thermophoresis effect.

Table 2 displays the effect of Casson rheological parameter, β on θ. As β increases, θ is escalated up to $\eta = 0.4$ and then it is declined for all values of Bi. **Table 3** portray that as Casson viscoplastic parameter β increases, both skin friction and Sherwood numbers are reduced whereas the Nusselt number, Nur is enhanced for any values of Bi. Overall significant effects are computed in the model with the inclusion of rheological, radiative and nanoscale effects, indicating that these effects are important to simulate in practical magnetorheological squeezing lubrication systems.

5. Concluding Remarks

Squeezing flow of a magnetorheological nanofluid with radiative heat transfer and viscous heating effects between parallel disks has been investigated theoretically using Fourier-type boundary conditions. Buongiorno's nanofluid model and Rosseland's diffusion flux approximation are deployed to analyse nanoscale and radiative effects. A nonlinear ordinary differential boundary value problem is derived using appropriate similarity transformation. Numerical solutions for the nonlinear system of differential equations were carried out by a MATLAB routine bvp4c. The MATLAB solutions have been verified for special cases in the literature. The simulations have shown that:

(i) Drag force in squeezing the fluid flow through the disks increases with greater magnetic field strength i.e. strong deceleration is induced.

(ii) Increasing squeezing parameter substantially modifies the velocity distribution causing a deceleration but an acceleration further from the disks.

(iii) Increasing the Brownian dynamics and thermophoresis parameters results in a boost in temperature and nanoparticle concentration.

(iv) Nanoparticle concentration is suppressed at the disk surfaces with increasing Brownian values.

(v) For suction and injection cases, the impact of all parameters on the temperature distributions are similar. However, opposite effects are computed for the concentration of the nanoparticles in comparison with the temperature.

(vi) With an increase in the Casson viscoplastic parameter, temperature decreases whereas nanoparticle concentration increases.

(vii) Increasing radiative parameter (i.e. weaker radiative flux and stronger thermal conduction contribution) depresses temperatures.

(viii) Elevation in Prandtl number, Eckert number and length parameter results in a significant enhancement in temperature but a strong depletion in nanoparticle concentration for both equal and unequal Biot numbers.

The present simulations have adopted a Casson viscoplastic formulation for the rheology of the magnetic nanofluid lubricant. Future investigations may address more complex non-Newtonian models e.g. micropolar models [65] and will be communicated imminently.

Conflict of Interest: The authors do not any conflict of interest

References

[1] İ. Çelik & H.K. Öztürk, Heat transfer and velocity in the squeezing flow between two parallel disks by Gegenbauer wavelet collocation method, *Archive of Applied Mechanics*, 91, 443–461, (2021).

[2] X. Kang *et al.*, Auxiliary bearing squeeze film dampers for magnetic bearing supported rotors, *Tribology International*, 146, 106181 (2020).

[3] H.McIClark, The influence of the squeeze film in slurry erosion, *Wear*, 256, 918-926, (2004)
.

[4] J. Zueco and O. Anwar Bég, Network numerical analysis of hydromagnetic squeeze film flow dynamics between two parallel rotating disks with induced magnetic field effects, *Tribology International*, 43, 532-543, (2010).

[5] N.B.Naduvinamani *et al.*, Squeeze film lubrication between circular stepped plates: Rabinowitsch fluid model, *Tribology International*, 73, 78-82, (2014).

[6] M.V. Bhat and G. M. Deberi, Squeeze film behaviour in porous annular discs lubricated with magnetic fluid, *Wear*, 151, 123-128, (1991).

[7] M.S. Lin *et al.,* Numerical and experimental study on the influence of material characteristics on the levitation performance of squeeze-film air bearing, *Tribology International*, 126, 307-316, (2018).

[8] K. Walters, The importance and measurement of lubricant rheology, *Tribology Series, 38*, 487-499, (2000).

[9] N. Ohno and F. Hirano, High pressure rheology analysis of traction oils based on free volume measurements, *Lubrication Engineering*, 57, 16–22, (2001).

[10] T. Hayat, H. Nazar, M. Imtiaz, A. Alsaedi, M. Ayub, Axisymmetric squeezing flow of third grade fluid in presence of convective conditions, *Chin J Phys*. 55, 738-54, (2017).

[11] L. Muravleva, Axisymmetric squeeze flow of a viscoplastic Bingham fluid, *J Non-Newtonian Fluid Mech.*, 249, 97-120, (2017).

[12] Y. Xu *et al.*, Squeeze flow behaviors of magnetorheological plastomers under constant volume, *J. Rheology*, 58, 659, (2014).

[13] N. Phan-Thien and W. Walsh, Squeeze-film flow of an Oldroyd-B fluid: Similarity solution and limiting Weissenberg number. *ZAMP*, 35, 747–759, (1984).

[14] 4. L. Muravlev, Axisymmetric squeeze flow of a Casson medium, J Nonnewton Fluid Mech. 267, 35-50, (2019).

[15] M. Shamshuddin, S.R. Mishra, Ali Kadir and O. Anwar Bég, Unsteady chemo-tribological squeezing flow of magnetized bioconvection lubricants: numerical study, *J. Nanofluids*, 8 (2019) 407-419.

[16] I. Çelik, H. K. Öztürk, Heat transfer and velocity in the squeezing flow between two parallel disks by Gegenbauer Wavelet Collocation Method, *Arch. Appl. Mech*., 91 (2021) 443–461.

[17] GH.R. Kefayati, FDLBM simulation of entropy generation due to natural convection in an enclosure filled with non-Newtonian nanofluid, *Powder Technology*, 273 (2015) 176-190.

[18] J.A. Aranda, Radiative heat transfer analysis of railroad bearings for wayside thermal detector optimization, MSc Thesis, University of Texas Rio Grande Valley, December (2018).

[19] F.D. Fischer, E. Werner, K. Knothe, The surface temperature of a half-plane subjected to rolling/sliding contact with convection. Trans. *ASME J. Tribol*. 122, 864 (2000).

[20] W.O. Winer, S. Bair, B. Gecim, Thermal resistance of a tapered roller bearing. *American Society of Lubrication Engineers*, 45, 8–10 (1985).

[21] J.C. Jeager, Moving sources of heat and the temperature at sliding contacts. Proc. R. Soc., 76**,** 203–224 (1942).

[22] B. Xu, C. W. Chia, Q. Zhang, Y. T. Toh, and C. An, Thermal analysis of heat-assisted magnetic recording optical head with laser diode on slider, *Jpn. J. Appl. Phys*. 50(9S1), 5M–9M (2011).

[23] J. B. Dahl and D. B. Bogy, Static and dynamic slider air-bearing behavior in heat-assisted magnetic recording under thermal flying height control and laser system-induced protrusion, *Tribol. Lett.* 54(1), 35–50 (2014).

[24] H. Wu, S. Xiong, S. Canchi, E. Schreck, and D. Bogy, Nanoscale heat transfer in the head-disk interface for heat assisted magnetic recording, *Appl. Phys. Lett.* 108(9), 093106 (2016).

[25] W. D. Zhou, B. Liu, S. K. Yu, W. Hua, and C. H. Wong, A generalized heat transfer model for thin film bearings at head-disk interface, *Appl. Phys. Lett*. **92**, 043109 (2008).

[26] S. T. Mohyud-Din, S. I. Khan, Nonlinear radiation effects on squeezing flow of a Casson fluid between parallel disks, *Aerospace Science and Technology*, 48 (2016) 186-192.

[27] S. I. Khan, U. Khan, N. Ahmed, S.T. Mohyud-Din, Thermal radiation effects on squeezing flow of Casson fluid between parallel disks, *Communications in Numerical Analysis* 2 (2016) 92-107.

[28] T. Hayat, S. Jabeen, A. Shafiq, A. Alsaedi, Radiative squeezing flow of second grade fluid with convective boundary conditions, *Plos One* 11 (2016) e0152555 1-22.

[29] GH.R. Kefayati, Simulation of heat transfer and entropy generation of MHD natural convection of non-Newtonian nanofluid in an enclosure, *Int. J. of Heat and Mass Transfer,* 92 (2016) 1066–1089.

[30] M. Bilal, Y. Urva**,** Analysis of non-Newtonian fluid flow over fine rotating thin needle for variable viscosity and activation energy, *Archive of Applied Mechanics*, 91 (2021) 1079–1095.

[31] K.R.V. Subramanian, Tubati Nageswara Rao and Avinash Balakrishnan, *Nanofluids and Their Engineering Applications*, CRC Press, Florida (2021).

[32] J. Buongiorno, Convective transport in nanofluids, *ASME J Heat Transfer*. 128 (2006) 240-50.

[33] Y. Hu *et al.,* Head flying characteristics in heat assisted magnetic recording considering various nanoscale heat transfer models, *Journal of Applied Physics*, 123, 034303 (2018).

[34] M. M. Hashmi, T. Hayat, A Alsaedi, On the analytical solutions for squeezing flow of nanofluid between parallel disks, *Nonlinear Anal Model Control*. 17 (2012) 418-430.

[35] GH.R. Kefayati, FDLBM simulation of mixed convection in a lid-driven cavity filled with non-Newtonian nanofluid in the presence of magnetic field, *Int. J.of Thermal Sciences*, 95 (2015) 29-46

[36] M. Hamid, M. Usman, R. Ul Haq and Z. Tian, A Galerkin approach to analyze MHD flow of nanofluid along converging/diverging channels, *Arch Appl Mech*, 91(2021) 1907–1924.

[37] S. Akram, A. Razia and F. Afzal, Effects of velocity second slip model and induced magnetic field on peristaltic transport of non-Newtonian fluid in the presence of double-diffusivity convection in nanofluids, *Archive of Applied Mechanics*, 90 (2020) 1583–1603.

[38] A. M. Aly, E. M. Mohamed, Numerical simulations of solid particles dispersion during double-diffusive convection of a nanofluid in a cavity with a wavy source, *Archive of Applied Mechanics*, 91 (2021) 2089–2108

[39] G.H.R. Kefayati, Natural convection of ferrofluid in a linearly heated cavity utilizing LBM,

Journal of Molecular Liquids 191 (2014) 1–9

[40] GH.R. Kefayati, Heat transfer and entropy generation of natural convection on non-Newtonian nanofluids in a porous cavity, *Powder technology*, 299 (2016) 127-149

[41] GH.R. Kefayati , FDLBM simulation of magnetic field effect on mixed convection in a two sided lid-driven cavity filled with non-Newtonian nanofluid, *Powder Technology*, 280 (2015) 135–153.

[42] F. A. Soomro, R. Ul Haq and M. Hamid, Brownian motion and thermophoretic effects on non-Newtonian nanofluid flow via Crank–Nicolson scheme, *Archive of Applied Mechanics,* 91 (2021) 3303–3313

[43] B. H. Rikitu, O. D. Makinde and L. G. Enyadene, Unsteady mixed convection of a radiating and reacting nanofluid with variable properties in a porous medium microchannel, *Archive of Applied Mechanics*, https://doi.org/10.1007/s00419-021-02043-8

[44] S.R.Afshar, S.R.Mishra, A. S. Dogonchi, Nader Karimi, A. J.Chamkha and HaniAbulkhair, Dissection of entropy production for the free convection of NEPCMs-filled porous wavy enclosure subject to volumetric heat source/sink, *Journal of the Taiwan Institute of Chemical Engineers*, 128 (2021) 98-113.

[45] A. S. Dogonchia, S.R. Mishra, N. Karimic, A. J. Chamkhad and H. Alhumade, Interaction of fusion temperature on the magnetic free convection of nano-encapsulated phase change materials within two rectangular fins equipped porous enclosure, *Journal of the Taiwan Institute of Chemical Engineers*, https://doi.org/10.1016/j.jtice.2021.03.010.

[46] A. J. Chamkha, A.S. Dogonchi, D.D. Ganji, Magnetohydrodynamic nanofluid natural convection in a cavity under thermal radiation and shape factor of nanoparticles impacts: A Numerical study using CVFEM, *Applied Science*, https://doi.org/10.3390/app8122396

[47] A.S. Dogonchia, S. M. Seyyedi , M. Hashemi-Tilehnoee, A. J. Chamkhac and D.D. Ganjie, Investigation of natural convection of magnetic nanofluid in an enclosure with a porous medium considering Brownian motion, *Case Studies in Thermal Engineering*, 14 (2019) 100502

[48] S. Shaw, A. S. Dogonchi, M. K. Nayak and O. D. Makinde, Impact of Entropy Generation and Nonlinear Thermal Radiation on Darcy–Forchheimer Flow of MnFe2O4-Casson/Water Nanofluid due to a Rotating Disk: Application to Brain Dynamics, *Arabian Journal for Science and Engineering*, https://doi.org/10.1007/s13369-020-04453-2

[49] S. M. Seyyedi, A. S. Dogonchi, D. D. Ganji and M. Hashemi-Tilehnoee, Entropy generation in a nanofluid-filled semi-annulus cavity by considering the shape of nanoparticles, *Journal of Thermal Analysis and Calorimetry*, https://doi.org/10.1007/s10973-019-08130-x

[50] M. H. Saidi, H. Tamim H, Heat transfer and pressure drop characteristics, of nanofluid in unsteady squeezing flow between rotating porous disks considering the effects of thermophoresis and Brownian motion, *Adv Powder Technol*. 27 (2016) 565-74.

[51] 3. N. Ahmed, U. Khan, S. T. Mohyud-Din, Influence of shape factor on flow of magneto-nanofluid squeezed between parallel disks, *Alex Eng J.* 57 (2018) 1893-903.

[52] K. Das, S. Jana, N. Acharya, Slip effects on squeezing flow of nanofluid between two parallel disks, *Int J Appl Mech Eng*. 21 (2016)5-20.

[53] O. Anwar Bég, Ayesha Sohail, T.A. Bég and A. Kadir, B-spline collocation simulation of nonlinear transient magnetic nano-bio-tribological squeeze film flow, *J. Mechanics in Medicine and Biology, 18, 1850007.1- 1850007.20 (20 pages) (2018).*

[54] M. G. Sobamowo, A. T. Akinshilo, On the analysis of squeezing flow of nanofluid between two parallel plates under the influence of magnetic field, *Alex Eng J*. (2017). https://doi.org/10.1016/j.aej. 2017.07.001

[55] I. Ullah, M. WAqas, T. Hayat, A. Alsaedi, M. Ijaz Khan, Thermally radiated squeezed flow of magneto-nanofluid between two parallel disks with chemical reaction, *J. of Thermal Analysis and Calorimetry*, 135, 1021–1030 (2019).

[56] N. U. Ahmed, S. I. Khan, Y. Xiao-Jun, Z.A. Zaidi, S. T. Mohyud-Din, Magnetohydrodynamic (MHD) squeezing flow of a Casson fluid between parallel disks, *International Journal of Physical Sciences*, 8 (2013) 1788-1799.

[57] U. Khan, S. I. Khan, N. Ahmed, S. Bano, S. T. Mohyud-Din, Heat transfer analysis for squeezing flow of a Casson fluid between parallel plates, *Ain Shams Engineering Journal* 7 (2016) 497-504.

[58] G. Janardhana Reddy, K. Bhaskerreddy, J. C. Umavathi, A. Mikhail Sheremet, Heat flow visualization for unsteady Casson fluid past a vertical slender hollow cylinder, *Thermal Science and Engineering Progress*. 5 (2018) 172-181.

[59] V.R. Prasad, A. SubbaRao, N. Bhaskar Reddy, B. Vasu, O. Anwar Bég, Modelling laminar transport phenomena in a Casson rheological fluid from a horizontal circular cylinder with partial slip, *Proc IMechE- Part E: J. Process Mechanical Engineering*, 227 (4) 309-326 (2013).

[60] J.C. Umavathi and O. Anwar Bég, Numerical study of double-diffusive dissipative reactive convective flow in an open vertical duct containing a non-Darcy porous medium with Robin boundary conditions, *J. Engineering Mathematics* (2019). https://doi.org/10.1007/ s10665-019-10022-w (13 pages)

[61] J.C. Umavathi and O. Anwar Bég, Mathematical modelling of triple diffusion in natural convection flow in a vertical duct with Robin boundary conditions, viscous heating and chemical reaction effects, *J. Engineering Thermophysics*, 29 (2020) 1–26.

[62] J. Kierzenka, and L. F. Shampine, A BVP solver based on residual control and the Matlab *PSE. ACM Transctions on Mathematical Software (TOMS)* 27 (2001) 299-316.

[63] T. Hayat, A. Yousaf, M. Mustafa and S. Obaidat, MHD squeezing flow of second grade fluid between two parallel disks, *Int. J. Numerical Methods in Fluids*, 69 (2012) 399-410.

[64] M.M. Hashmi, T. Hayat and A. Alsaedi, On the analytic solutions for squeezing flow of Nanofluids between parallel disks, Nonlinear Analysis: Modelling and Control, 17 (2012) 418-430.

[65] G.M. Abdel-Rahman, Studying effect of MHD on thin films of a micropolar fluid, *Physica B: Condensed Matter*, 404, 3859-3866 (2009).

Appendix

The rheological equation of the Casson fluid is defined (following Mohyud-Din and Khan [26], and Khan et al. [27]) as follows:

$$\tau_{ij} = \left[\mu_B + \left(\frac{p_y}{2\pi} \right)^{1/n} \right]^n 2\, e_{ij} \tag{A1}$$

where μ_B dynamic viscosity of the non-Newtonian fluid, p_y is yield stress of the fluid and π is the product of the component of deformation rate with itself, i.e., $\pi = e_{ij}\, e_{ij}$,(self-product of component of deformation rate with itself) where e_{ij} is the $(i, j)^{th}$ component of the deformation rate. For $n< 1$ the fluid is pseudoplastic (shear-thinning), for $n > 1$ it is dilatant (shear-thickening). Further:

$$\tau_{ij} = \begin{cases} 2 e_{ij} \left[\frac{p_y}{\sqrt{2\pi}} + \mu_B \right] & \pi > \pi_c \\ 2 e_{ij} \left[\frac{p_y}{\sqrt{2\pi_c}} + \mu_B \right] & \pi < \pi_c \end{cases} \tag{A2}$$

Here π_c is the critical value of the said self-product. If shear stress is less than the yield stress applied to the fluid, the fluid acts like a solid, whereas if shear stress exceeds the yield stress, motion is initiated. Examples of Casson fluid are jelly, foodstuffs, tomato sauce, gels, honey, certain polymers, soup, blood under certain shear rates, etc.